

# A single particle multichannel bio-aerosol fluorescence sensor

P. H. Kaye, W. R. Stanley and E. Hirst

*Science & Technology Research Institute, University of Hertfordshire, Hatfield, Herts. AL10 9AB, U.K.  
[p.h.kaye@herts.ac.uk](mailto:p.h.kaye@herts.ac.uk)*

E.V. Foot, K. L. Baxter and S. J. Barrington

*Defence Science & Technology Laboratory, Porton Down, Salisbury, Wilts. SP4 0JQ, U.K.*

**Abstract:** We describe a prototype low-cost multi-channel aerosol fluorescence sensor designed for unattended deployment in medium to large area bio-aerosol detection networks. Individual airborne particles down to  $\sim 1\mu\text{m}$  in size are detected and sized by measurement of light scattered from a continuous-wave diode laser (660nm). This scatter signal is then used to trigger the sequential firing of two xenon sources which irradiate the particle with UV pulses at  $\sim 280\text{ nm}$  and  $\sim 370\text{ nm}$ , optimal for excitation of bio-fluorophores tryptophan and NADH respectively. For each excitation wavelength, fluorescence is detected across two bands embracing the peak emissions of the same bio-fluorophores. Current measurement rates are up to  $\sim 125$  particles/s, corresponding to all particles for concentrations up to  $1.3 \times 10^4$  particles/l. Developments to increase this to  $\sim 500$  particles/s are in hand. Device sensitivity is illustrated in preliminary data recorded from aerosols of E.coli, BG spores, and a variety of non-biological materials.

© 2005 Optical Society of America

**OCIS codes:** (120.0120) Instrumentation; (010.1100) Aerosol Detection; (260.2510) Fluorescence.

---

## References and links

1. R.G. Pinnick, S.C. Hill, P. Nachman, J.D. Pendleton, G.L. Fernandez, M.W. Mayo, and J.G. Bruno, "Fluorescent particle counter for detecting airborne bacteria and other biological particles", *Aerosol Sci. Technol.* **23**, **4**, 653-664 (1995).
2. P.P. Hairston, J. Ho, and F.R. Quant, "Design of an instrument for real-time detection of bioaerosols using simultaneous measurement of particle aerodynamic size and intrinsic fluorescence", *J. Aerosol Sci.* **28**, **3**, 471-480 (1997).
3. G. Chen, P. Nachman, R. G. Pinnick, S. C. Hill, and R. K. Chang, "Conditional-firing aerosol-fluorescence spectrum analyzer for individual airborne particles with pulsed 266-nm laser excitation," *Opt. Lett.* **21**, 1307-1309 (1996).
4. M. Seaver, J. D. Eversole, J. J. Hardgrove, W. K. Cary, Jr., and D. C. Roselle, "Size and fluorescence measurements for field detection of biological aerosols," *Aerosol Sci. Technol.* **30**, 174-185 (1999).
5. F.L. Reyes, T. H. Jeys, N. R. Newbury, C. A. Primmerman, G. S. Rowe, and A. Sanchez, "Bio-aerosol fluorescence sensor", *Field Anal. Chem. and Technol.* **3**(4-5), 240-248 (1999).
6. Y-L Pan, S. Holler, R. K. Chang, S. C. Hill, R. G. Pinnick, S. Niles and J. R. Bottiger, "Single-shot fluorescence spectra of individual micrometer-sized bioaerosols illuminated by a 351- or 266-nm ultraviolet laser," *Opt. Lett.* **24**, 116-119 (1999).
7. Y-L Pan, P. Cobler, S. Rhodes, A. Potter, T. Chou, S. Holler, R. K. Chang, R. G. Pinnick, J-P Wolf, "High-speed, high-sensitivity aerosol fluorescence spectrum detection using a 32-anode photomultiplier tube detector", *Rev. Sci. Instrum.* **72**, **3**, 1831-1836 (2001).
8. Y-L Pan, J. Hartings, R. G. Pinnick, S. C. Hills, J. Halverson and R. K. Chang, "Single particle fluorescence spectrometer for ambient aerosols", *Aerosol Sci. Technol.*, **37**, 628-639 (2003).
9. P.H. Kaye, J.E. Barton, E. Hirst, and J.M. Clark; "Simultaneous light scattering and intrinsic fluorescence measurement for the classification of airborne particles". *Applied Optics* **39**, **21**, 3738-3745 (2000).

10. V. E. Foot, J. M. Clark, K. L. Baxter, and N. Close, "Characterising single airborne particles by fluorescence emission and spatial analysis of elastic scattered light", in *Optically Based Biological and Chemical Sensing for Defence*. J. C. Carrano and A. Zukauskas, eds. Proc. SPIE **5617**, 292-299 (2004).
  11. SUVOS – Semiconductor Ultraviolet Optical Sources, J. C. Carrano, director, <http://www.darpa.mil/mto/suvos/> (2002).
  12. T.H. Jeys, L. Desmarais, E. J. Lynch, and J.R. Ochoa, "Development of a UV LED based biosensor", in *Sensors and Command, Control, and Intelligence Technologies for Homeland Defense and Law Enforcement*. E.M. Carrapezza, ed. SPIE **5071**, 234-240 (2003).
  13. P. H. Kaye, E. Hirst, V. E. Foot, J. M. Clark and K. Baxter, "A low-cost multichannel aerosol fluorescence sensor for networked deployment", in *Optically Based Biological and Chemical Sensing for Defence*. J. C. Carrano and A. Zukauskas, eds. Proc. SPIE **5617**, 388-398 (2004).
  14. C. F. Bohren and D. R. Huffman, *Absorption and Scattering of Light by Small Particles* (Wiley, New York, 1983).
- 

## 1. Introduction

In the search for methods by which an ambient environment can be continuously monitored for potentially harmful biological aerosols, particle fluorescence methods have received considerable attention over the past decade. When excited by radiation tuned to the principal biological fluorophores contained within biological organisms, intrinsic particle fluorescence can be used to help differentiate biological from non-biological particles and can even provide some discrimination between biological particles which are normal constituents of an ambient environment and those which may be considered a threat.

However, because intrinsic fluorescence from biological fluorophores is generally weak, and because the fluorophores in airborne biological particles are normally present in extremely small quantities, the exciting radiation must be intense, and lasers have commonly been employed for this purpose. In the earliest systems, continuous wave lasers were employed, for example [1,2], though these were usually large and fragile and operated at wavelengths which were too long for efficient excitation of some of the important bio-fluorophores such as tryptophan, for which optimal excitation occurred at wavelengths of ~260-280 nm. Hence the use of various solid-state lasers employing harmonic generation, such as frequency quadrupled Nd-YAG lasers, has gained acceptance [eg. 3-10], both for the output wavelength of 266nm and because they offered a generally smaller form-factor than continuous-wave gas lasers.

### 1.1 Laser Induced Fluorescence

These developments have helped realise the potential of laser-induced fluorescence (LIF) for the characterization of individual airborne particles and the potential detection of pathogens. However, solid-state harmonic lasers are relatively expensive components to be incorporated in systems where multiple-point detection or widespread field monitoring may be required. Because of this, considerable effort is presently going into the development of compact and robust semiconductor sources capable of delivering continuous wave sub-300 nm radiation. In particular, the US SUVOS (Semiconductor Ultraviolet Optical Sources [11]) programme, which commenced in 2002, is making significant gains towards this objective and has already demonstrated prototype LED (light emitting diode) devices capable of room temperature continuous 280nm emission at milliwatt power levels. These devices have already been incorporated in a test-bed sensor for bioaerosols [12].

Published results from existing particle LIF systems developed over the past decade allows determination of an approximate lower limit of 'fluorescence excitation and capture' for the satisfactory generation and recording of LIF from typical individual biological particles of interest. This shows that, in general, a particle must experience a UV fluence greater than ~200-300  $\mu\text{J}/\text{cm}^2$  for each steradian of fluorescence collection angle for adequate signal-to-noise in the acquired signal. Where higher resolution spectral information is required, the fluence must be proportionally higher; for example, Yong-Le Pan [8] describes a fluorescence spectrometer with more than 100 recording channels in which a UV fluence of  $\sim 3 \times 10^4 \mu\text{J}/\text{cm}^2$  is used.

The required UV energy may be delivered to the particle in tens of nanoseconds, as from a Q-switched solid-state laser, or for continuous-wave lower power sources such as UV LEDs, over millisecond timeframes. However, in the latter case the need to retain a single particle within the focused UV beam for such relatively long periods can be problematic and can compromise overall aerosol sample volumetric flow rate.

Therefore, while UV LEDs and ultimately UV diode lasers undoubtedly offer the best prospects for practical bio-aerosol fluorescence sensors, device output powers and lifetimes must be increased before they can be incorporated into commercial field detection systems. Until such devices are routinely available, alternative low-cost high-irradiance UV sources must be sought to help meet the pressing need for affordable fluorescence-based bio-aerosol sensors in military and civilian scenarios. Miniature xenon flashtubes represent one such alternative, being capable of delivering the required UV fluence to the particle and, as broadband sources, offering selection of optimal excitation wavelengths for biological fluorophore excitation. This paper describes a compact low-cost prototype aerosol fluorescence sensor that employs two such xenon flashtubes to record two-channel fluorescence emission data from individual airborne particles down to  $\sim 1\mu\text{m}$  in size at rates up to  $\sim 7,500$  particles per minute.

## 2. Single particle aerosol fluorescence sensor, WIBS2.

The prototype described here is based on an earlier dual-xenon Wide Issue Bio-aerosol Sensor, WIBS [13] that recorded fluorescence emission from multiple particles present within a large sample volume of several  $\text{cm}^3$  upon the periodic flashing of two optically filtered xenon sources. Such simultaneous multiple particle illumination greatly simplified mechanical airflow systems and detection optics, making the overall sensor very low cost. However, this was offset by the limitation that simultaneous excitation of multiple particles would inevitably result in fluorescence data averaged over all particles, and whilst this was acceptable for broadly homogeneous aerosols, it compromised the ability of the sensor to differentiate low concentrations of potentially harmful biological particles against a higher concentration of background particles. Measurement of individual particles was necessary to avoid this.

### 2.1 Overview of WIBS2 operation

The new *single-particle* fluorescence sensor, WIBS2, employs a central optical chamber around which are arranged a continuous-wave 660nm diode laser used in the detection and sizing of particles (see section 2.4), two pulsed xenon UV sources emitting at different wavebands (see section 2.3), and two fluorescence detection channels, FL1 and FL2, detecting intrinsic particle fluorescence across two wavebands. Thus, for each particle, a 2x2 excitation-emission matrix is recorded along with an estimate of particle size.

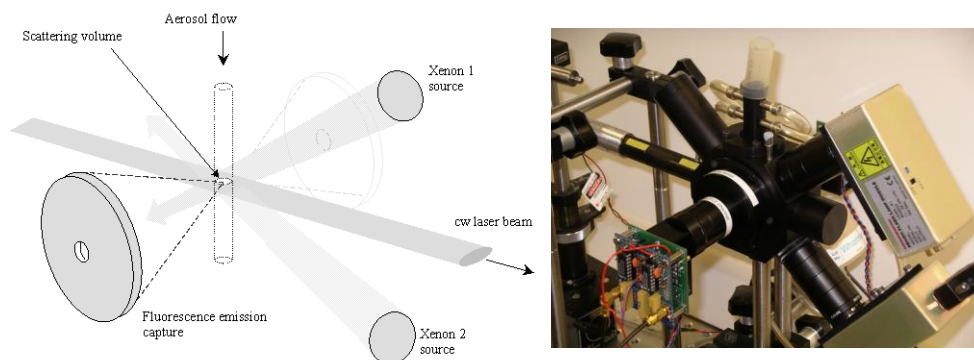


Fig. 1. Schematic layout of WIBS2 sensor and the actual sensor itself, approximately (26x22x28) cm in size.

In operation, aerosol is drawn from the ambient atmosphere via a laminar-flow delivery system which renders suspended particles in essentially single file as they traverse the focused beam from the diode laser at the centre of the chamber. Total aerosol flow is 4.5 l/min, of which 3.9 l/min is filtered before being re-introduced to form a sheath flow confining the remaining sample flow. The intersection of this aerosol sample flow and laser beam defines the *scattering volume*, ~ 0.8 mm diameter and 130  $\mu\text{m}$  depth, as indicated in Fig. 1.

Each particle entering the laser beam produces a scattered light signal from which an estimate of particle (spherical equivalent) size is determined from Mie theory [14]. Particles deemed greater than ~1  $\mu\text{m}$  in size initiate the sequential firing of the two xenon UV sources: the first xenon, Xe1, fires 10  $\mu\text{s}$  after particle detection, by which time the particle has moved ~180  $\mu\text{m}$  to just below the laser beam; the second xenon, Xe2, fires 5  $\mu\text{s}$  later and is aimed marginally lower than the first to account for the additional particle movement during this time.

At the point of intersection with the scattering volume, the UV radiation pulse from each xenon is approximately 2 mm by 1 mm in cross-section (see Fig. 2) and illuminates the entire scattering volume with an essentially uniform fluence in excess of ~300  $\mu\text{J}/\text{cm}^2$ . Wherever the particle passes through the scattering volume, it therefore experiences similar UV excitation fluence (to within ~ $\pm 6\%$ ), an important consideration when comparing the fluorescence properties of different particle types.

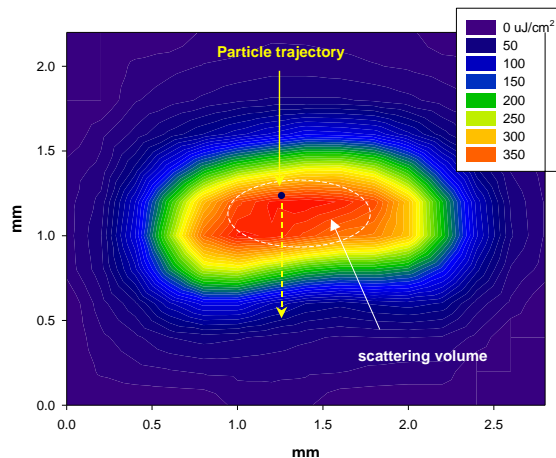


Fig. 2. Cross-section of xenon UV pulse superimposed on the *scattering volume* (dotted ellipse) as viewed from the xenon source.

WIBS2 uses two Hamamatsu L9455 xenon modules (Hamamatsu Photonics K.K., Japan). These are compact (10 x 4 x 3.5cm), externally-triggerable modules which incorporate a precision xenon discharge tube with an arc length of 1.5 mm. Flash-to-flash energy reproducibility is better than  $\pm 3\%$  (though in WIBS2 each individual discharge is measured and correction made for variations). The xenon sources operate with a maximum discharge energy (electrical) of 40 mJ and a flash duration of ~1  $\mu\text{s}$ . At this maximum flash energy, the maximum repetition rate for the xenons is 126 Hz, set by the unit's thermal dissipation limit of 5 W. With its current sample flow-rate of 0.6 l  $\text{min}^{-1}$ , WIBS2 is therefore capable of exciting fluorescence in all particles for particle concentrations up to  $\sim 1.3 \times 10^4$  particles/l. Beyond this concentration, the additional particles are counted and sized only.

Xenon output decreases slowly with pulse number, falling to ~75% of maximum after  $\sim 1.5 \times 10^9$  pulses, equivalent to approximately 3,000 hours of continuous operation at the maximum discharge rate of 126 Hz. For ambient particle concentrations lower than  $\sim 1.3 \times 10^4$  particles/l, useable xenon lifetime will be proportionally longer.

## 2.2 Fluorescence collection

Intrinsic fluorescence emission from the particle excited by the two xenon UV pulses is collected via detection channels FL1 and FL2. Each channel comprises an apertured 51mm diameter spherical mirror of 17.5 mm focal length (01 MCG 013, Melles Griot Inc.) that reflects the fluorescent light emanating from the particle back across the chamber to the aperture in an identical opposing mirror, as shown in the Zemax™ ray diagram, Fig. 3. Each mirror thus collects fluorescence emission over a solid angle of  $\sim 3.1$  sr and directs it to the photocathode of a miniature photomultiplier (PMT) module (H6779, Hamamatsu Inc.) via a band-pass filter, as described in Section 2.3. The optical design of the system is such that the field-of-view of the PMT is restricted to a region only marginally larger than the scattering volume. This reduces the probability of the PMT receiving unwanted fluorescence light from, for example, a second particle closely following the first and experiencing UV irradiance in the periphery of the  $2 \times 1$  mm xenon pulse field.

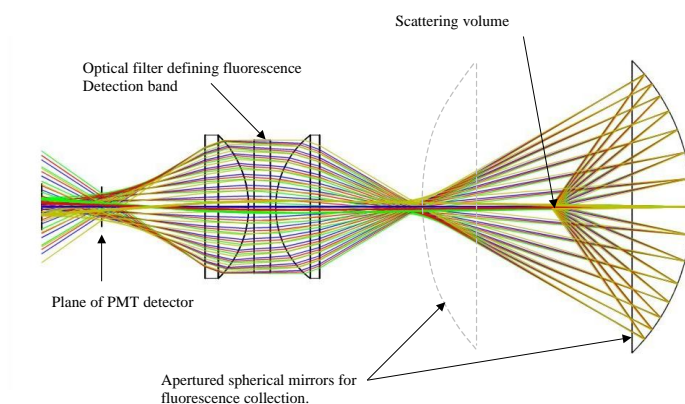


Fig. 3. Ray diagram showing fluorescence collection for one fluorescence detection channel (Mirror for second channel shown as dotted line).

## 2.3 Fluorescence excitation and emission bands

The output of the first xenon, Xe1, is optically filtered using a custom UV bandpass filter (SPUV280, Envin Scientific Ltd, Tattenhall, England). This results in radiation of peak wavelength  $\sim 280$  nm (Fig. 4), matched to the absorption peak of the biological fluorophore tryptophan, an amino acid common to organisms such as bacteria. The second xenon, Xe2, is filtered using an off-the-shelf bandpass filter (DUG11 UV, Schott AG, Mainz, Germany) to produce radiation (as in Fig. 4, right) with a peak close to the  $\sim 370$ nm absorption maximum of another important biological fluorophore, NADH (nicotinamide adenine dinucleotide).

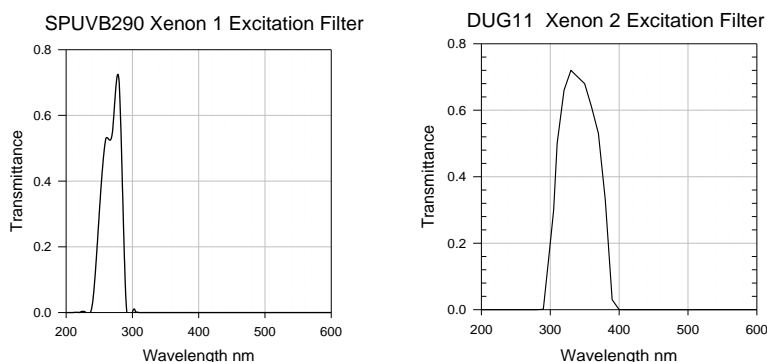


Fig. 4. Spectral outputs of the WIBS2 xenon sources Xe1 and Xe2

The first fluorescence detection channel, FL1, is required to measure fluorescence across a band coinciding with the maximum of the emission spectrum of tryptophan, ie: approximately 300-420 nm, peaking at ~345 nm. A custom long-pass optical filter (DUV2, Envin Scientific Ltd, Tattenhall, England) offering a 50% transmittance at ~330 nm was originally employed for this purpose. When combined with the roll-off in responsivity of the photomultiplier photocathode, a detection band extending from ~320-600 nm is produced, as shown in Fig. 5.

The second detection channel, FL2, is targeted towards the NADH emission band, ie: ~400-600 nm, peaking at ~450 nm. This waveband definition was achieved using a standard KV418 filter (Schott AG, Mainz, Germany), a high pass filter with sharp cut-off and very low intrinsic fluorescence. Again, the combination of this filter's transmittance and the roll-off in responsivity of the photomultiplier photocathode effectively defined the required band, as in Fig. 5.

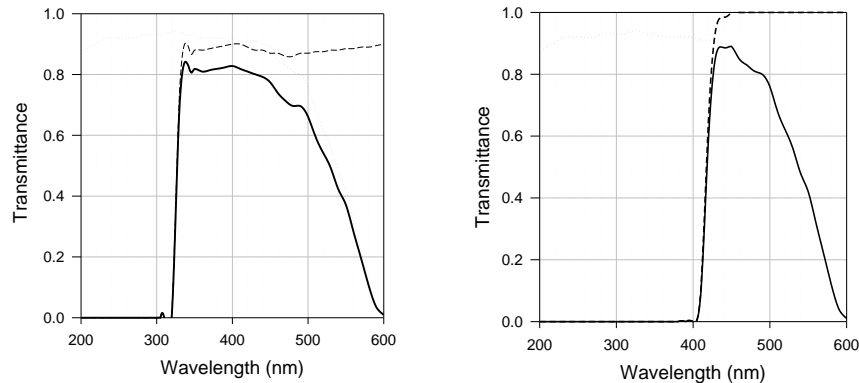


Fig. 5. Fluorescence detection bands for FL1 (left) and FL2 (right) channels. In each case, the dotted line represents the responsivity of the PMT detector, the dashed line the long-pass filter used, and the solid line the resultant fluorescence pass-band.

Whilst the FL1 band extends far beyond the upper limit of the primary tryptophan emission peak at approximately 420 nm, it is the *difference* between this transmission and that of the FL2 channel that embraces the majority of the band associated with tryptophan emission. (Note that, whilst the experimental data given in this paper were recorded with the filter configuration as shown in Fig. 5., a new long-pass filter having a 50% transmittance of ~310 nm will shortly replace the DUV2 long-pass filter in the FL1 channel. This will offer an 40% improvement in the efficient capture of the short-wavelength tryptophan fluorescence emission peak).

#### 2.4 Particle Detection

As mentioned above, the entry of a particle into the scattering volume is detected via the light scattered elastically from the cw diode laser beam. For convenience and to further reduce sensor unit cost, this scattered light detection is also achieved by the FL2 fluorescence detection channel. As indicated in Fig. 5, the photomultiplier detector used in the FL2 channel has a responsivity that falls off rapidly towards 600 nm wavelength. At the 660 nm wavelength of the laser, the PMT responsivity is a factor of  $\sim 10^3$  down on its peak value at ~400 nm. Fortunately, the magnitude of the elastically scattered signal from the particle is often a similar factor *larger* than the particle fluorescence, and this allows both the elastic scatter and FL2 fluorescence pulse (which, of course, occur at different times) to be successfully recorded using the same PMT gain setting. See section 2.5 below.

## 2.5 Data acquisition

The cycle for acquiring size and fluorescence data from the particle takes approximately 25  $\mu\text{s}$ . Fig. 6 shows oscilloscope waveforms of the signals from detector channels FL1 and FL2 when a 3  $\mu\text{m}$  diameter polystyrene latex sphere passes through the scattering volume.

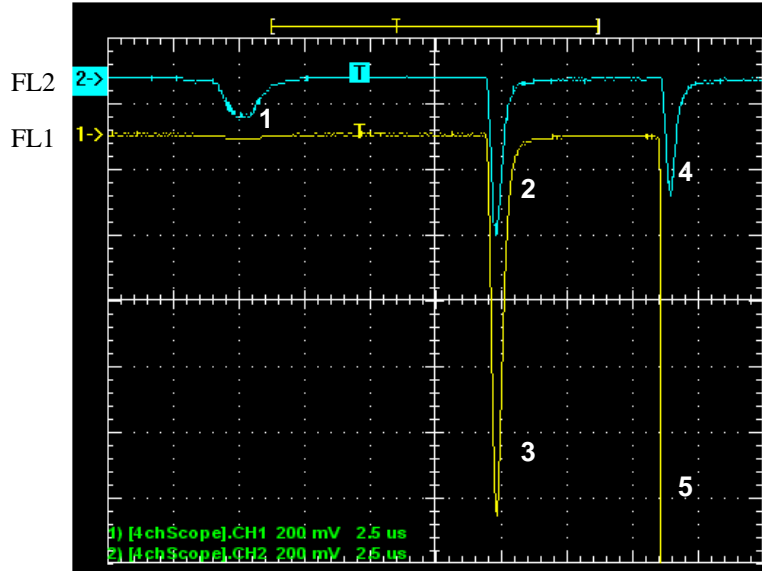


Fig. 6. Example of FL1 and FL2 detector signals resulting from the passage of a 3  $\mu\text{m}$  PSL sphere through the scattering volume. (See text for explanation of numbering).

When the particle enters the laser beam, the FL2 channel (upper trace) records the magnitude of the elastic scatter signal, numbered (1), as negative going signal. (The FL1 trace also detects this scattered light signal, though at a smaller magnitude because the gain of the FL1 channel is set lower than that for FL2; see Section 3 below).

Some 10  $\mu\text{s}$  after particle detection, the Xe1 xenon fires, illuminating the particle with  $\sim 280$  nm UV radiation and producing the fluorescence signals (2) and (3) from channels FL2 and FL1 respectively. Some 5  $\mu\text{s}$  after this, Xe2 fires, illuminating the particle with  $\sim 370$  nm UV radiation. Channel FL2 records the fluorescence emission (4) from the particle at wavelengths within its pass-band of  $\sim 420$ -600 nm. However, the Xe2 radiation lies *within* the pass-band of channel FL1 and therefore the PMT in this channel receives the *elastic scatter* from the particle. The magnitude of the elastically scattered  $\sim 370$  nm radiation is far higher than the fluorescence signal it excites and is sufficient to momentarily saturate the detection amplifier on the FL1 channel. This saturated signal pulse (5) is thus discarded. Recovery of the amplifiers from saturation takes a further  $\sim 10$   $\mu\text{s}$ .

Signals (1), (2), (3), and (4) are integrated over their width and the integrated values digitised to 12-bit accuracy before being passed to a host processor. The system is now ready to detect a further particle. However, since the xenon sources require approximately 5 ms to re-charge, any particles passing through the scattering volume during this 5 ms period are sized and recorded, but no fluorescence data is acquired.

## 2.6 Data processing

The fluorescence data recorded from each particle must be corrected for the following (in decreasing order of importance):

- i. Background offsets: i.e. a small contribution to the signals detected by FL1 and FL2 caused by both low-level fluorescence excited by stray UV in the scattering chamber

and filter breakthrough arising from the extremely small but finite filter transmittance in the ‘stop-bands’. The magnitudes of these offsets are determined by measuring the FL1 and FL2 channel responses when the Xe1 and Xe2 xenons are forced to fire under conditions of no sample flow and no particle in the scattering volume.

- ii. Small pulse-to-pulse variability in UV pulse energy and long-term reduction in pulse energy. This is facilitated by recording the magnitude of each UV pulse from Xe1 and Xe2 using UV-sensitive photodiodes.
- iii. Filter fluorescence. The optical filters in the FL1 and FL2 channels are bombarded with elastically scattered UV from the particle as well as fluorescent light. For sufficiently high-magnitude scattered UV, detectable levels of filter fluorescence are produced. Correction of this effect is achieved by recording the level of apparent ‘fluorescence’ from known non-fluorescent particles of quartz or sodium chloride and determining a factor for the ‘filter fluorescence’ per unit particle ‘size’.

The data presented in the following section have been corrected for the above sources of error.

### 3. Preliminary experimental data

Table 1. Notation used in WIBS2 data analysis.

Notation	Excitation	Fluorescence detection
FL1Xe1	~280 nm	~320 – 600 nm
FL2Xe1	~280 nm	~420 – 600 nm
FL2Xe2	~370 nm	~420 – 600 nm

There are numerous potential methods of combining the three ‘fluorescence’ metrics listed in Table 1 together with particle size and particle number concentration. Whilst simple graphical representations as presented below are informative, other methods based on, for example, artificial neural network analysis, are more amenable to automated decision making and are being pursued by our co-authors at DSTL.

Fig. 7 shows results recorded from a variety of test aerosols of some common fluorescent and non-fluorescent materials selected to help establish the degree of particle discrimination that WIBS2 may achieve. The polystyrene latex sphere samples were aerosolised using a TSI TriJet Aerosol Generator (TSI Inc, St. Paul, MN) into a 100 litre ballast chamber from which the sample was drawn. The dry powder materials: paper mulberry pollen, gypsum fibres, kettle scale ( $\text{CaCO}_3$ ) fibres, and cornflour (called cornstarch in the USA), were aerosolised directly into the ballast chamber using a filtered compressed-air supply. The ‘Tonic Water’ (actually 1% proprietary tonic water in distilled water) was sprayed directly into the ballast chamber.

In Fig. 7, the x-axis ‘Size’ is in arbitrary units; no attempt has been made here to convert the recorded particle scatter data to a spherical equivalent particle size though the scale extends approximately from ~0.5 to 10  $\mu\text{m}$ . The y-axis ‘FL2Xe2’ fluorescence signal is again in arbitrary units. The z-axis ‘FL1Xe1/FL2Xe1’ is a dimensionless quantity that is primarily a function of the particle material alone, reflecting as it does the spectral distribution of the fluorescence emission rather than its absolute magnitude. If the gains of the FL1 and FL2 photomultipliers were equal, the ratio FL1Xe1/FL2Xe1 would almost always exceed unity (see transmittance curves in Fig. 5). However, for many materials, the fluorescence emission in the 300-400 nm band can be significantly larger than that above 400 nm, and so, to

maximise dynamic range, the gain of the FL1 PMT is set an order of magnitude lower than that of channel FL2.

Fig. 7 and the associated QuickTime movie file show that, for the somewhat diverse aerosol types, discrimination is readily achieved in most cases. The distribution for the 1  $\mu\text{m}$  polystyrene latex spheres (Duke Scientific Inc) is wider than that of the 3  $\mu\text{m}$  and 5  $\mu\text{m}$  variants of the same material, a result of the lower signal-to-noise in the scatter and fluorescence signals for these smallest particles. Similarly, the gypsum and kettle scale particles exhibit relatively widespread distributions since their extremely low fluorescence (and hence low S/N ratios) can yield large variations in the FL1Xe1/FL2Xe1 ratio. Both the Tonic Water (1% in distilled water) droplets and the fluorescently doped 1.7  $\mu\text{m}$  latex spheres produce, as expected, high values of fluorescence, especially in the 420 – 600 nm band covered by the FL2 channel.

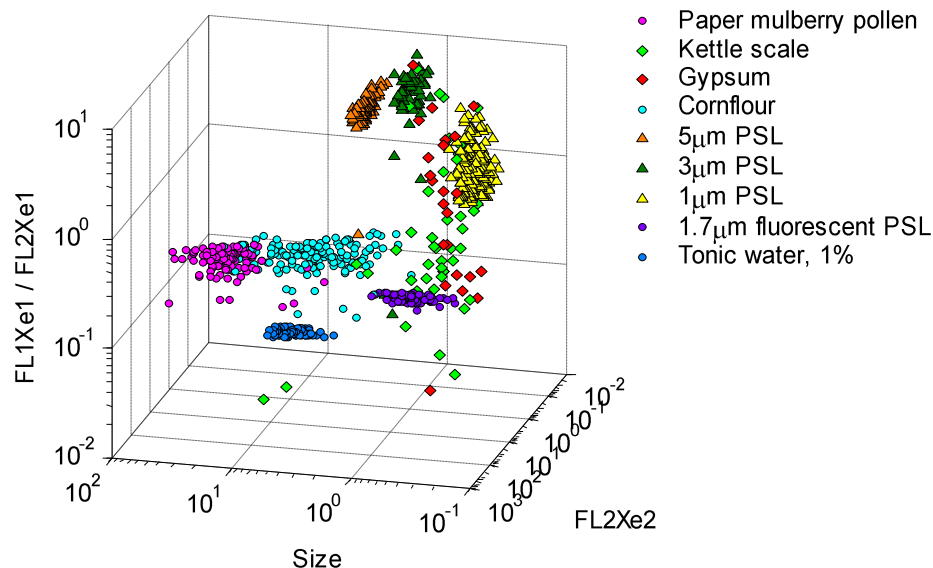


Fig. 7. (2.1 MB) Movie of preliminary WIBS2 data from test aerosol materials.

### 3.1 Biological aerosols

Fig. 8 shows results from aerosols more representative of the type of biological materials and organisms which a prospective bio-aerosol sensor would need to be able to detect and, ideally, discriminate. These data, recorded at DSTL Porton Down, UK, show results from aerosols of: washed BG spores (*Bacillus atrophaeus*, a simulant of *B. anthracis* spores); dry dispersed non-viable BG spores; washed and unwashed *E. coli* (*Escherichia coli*) vegetative cells; 0.1 mmol solutions of tryptophan and NADH (both in 1% sucrose solution); a 1% solution of ovalbumen in water; and 3  $\mu\text{m}$  latex spheres. For reference, the data relating to 1% Tonic Water and 1.7  $\mu\text{m}$  fluorescent latex spheres are reproduced here from Fig. 7. With the exception of the dry BG spores which were aerosolised using filtered compressed air, each material was nebulised from liquid suspension. All aerosols were generated into a large containment chamber incorporating a recirculation fan and from which the sample was drawn into the WIBS2 sensor. Parallel sampling of the aerosol by an aerodynamic particle sizer (TSI APS 3300) provided data relating to aerosol concentration and mean particle size.

The data in Fig. 8 show that promising degree of discrimination between the various particle types. Of note are:

- i. The distributions of the washed and dry dispersed BG spores appear relatively coincident despite their differing material state. The mean particle size of the washed spore distribution as recorded by the APS was  $\sim 1.1 \mu\text{m}$ ; the distribution of the dry

- dispersed spores exhibited a larger mean of  $\sim 1.5 \mu\text{m}$  with a tail extending out to  $\sim 5 \mu\text{m}$ , indicating the occurrence of some spore aggregates.
- ii. The E.coli washed and unwashed cells resulted in two distinct distributions, both exhibiting a  $\sim 1\text{-}2 \mu\text{m}$  size range. The washed cells distribution occurs at higher values of FL1Xe1/FL2Xe1 than the BG spore data, suggesting an increased level of fluorescence for the E.coli vegetative cells in the 320-420 nm band. The unwashed cell data are at a lower level of FL1Xe1/FL2Xe1 and a higher value on the FL2Xe2 axis, both consistent with increased longer wavelength fluorescence caused by residual growth media on the cells.
  - iii. Several aerosol data distributions, for example, for particles of E.coli and unwashed BG spores, show a consistent trend of increasing FL2Xe2 and decreasing FL1Xe1/FL2Xe1 with increasing size. This is postulated to be caused by possible re-absorption of short-wavelength fluorescence within the larger particles, though further investigation is required.
  - iv. The ovalbumen and tryptophan distributions are essentially coincident at high values of FL1Xe1/FL2Xe1, a consequence of their similar strong fluorescence properties in the  $\sim 300 - 450 \text{ nm}$  band.

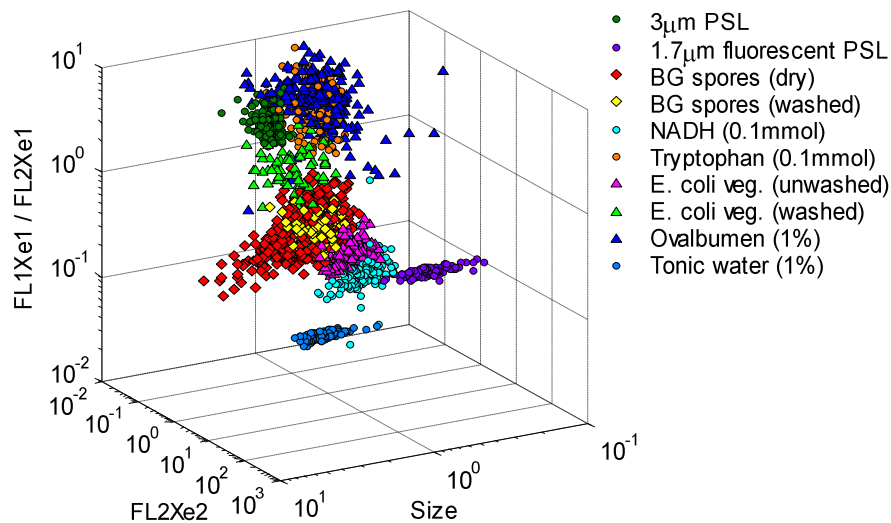


Fig. 8. (2.38 MB) Movie of WIBS2 preliminary data recorded from a variety of biological and non-biological aerosols.

#### 4. Conclusions

The dual-xenon WIBS2 prototype has demonstrated its potential for the discrimination of biological and non-biological aerosol particles down to  $\sim 1 \mu\text{m}$  in size. Further refinements are in hand which will allow the maximum particle analysis rate to be increased to  $\sim 500$  particles/s and the sample flow-rate increased to  $\sim 1 \text{ l/min}$ .

Whilst semiconductor UV LED and laser diode UV sources may ultimately offer the best solution for particle fluorescence excitation once sufficient device lifetimes and output powers have been achieved, the use of precision xenon UV sources such as those described here may help meet the present civilian and military requirement for low-cost field-based bio-aerosol detection.

#### Acknowledgements

This work was carried out under support from the Defence Science and Technology Laboratory, Porton Down, U.K.